# Near-surface solute redistribution during evaporation

M. Bechtold, <sup>1,2</sup> S. Haber-Pohlmeier, <sup>3</sup> J. Vanderborght, <sup>1</sup> A. Pohlmeier, <sup>1</sup> T. P. A. Ferré, <sup>4</sup> and H. Vereecken <sup>1</sup>

Received 20 May 2011; revised 1 August 2011; accepted 4 August 2011; published 7 September 2011.

[1] We present results from solute transport experiments in an evaporating composite porous medium consisting of a cylindrical inner core with coarse sand that was surrounded by a mantle with fine sand. Small volumes of dye and salt tracer were applied at the surface of the fine material of the evaporating column. The pressure head at the bottom boundary was kept constant using a hanging water table ensuring liquid phase continuity to top surface in both fine and coarse material, whereby the latter was hydraulically less conductive at these pressure conditions. Contrary to the expectation that solute accumulation at an evaporating surface is proportional to local cumulative evaporation, high concentration spots developed at the surface of the coarse material, for which IR surface temperature measurements did not indicate higher evaporation fluxes. 3D unsaturated flow and transport simulations and a second tracer experiment monitored with magnetic resonance imaging (MRI) demonstrated that preferential upward water flux in the fine sand deeper in the column and near-surface lateral water flow from the fine into the coarse sand in combination with a downward diffusive flux are responsible for the local solute accumulation. We propose that at the wet regions of a soil surface, solute accumulation is largely decoupled from local evaporation fluxes and strongly governed by relative differences of the hydraulic conductivities. The possible formation of high solute concentration spots at the surface of coarser regions usually representing preferential flow pathways during strong precipitation may have an accelerating effect on the leaching of solutes. Citation: Bechtold, M., S. Haber-Pohlmeier, J. Vanderborght, A. Pohlmeier, T. P. A. Ferré, and H. Vereecken (2011), Near-surface solute redistribution during evaporation, Geophys. Res. Lett., 38, L17404, doi:10.1029/ 2011GL048147.

#### 1. Introduction

[2] Quantifying solute migration through soil is critical for understanding nutrient cycling and soil/atmosphere mass flux and for managing soil and groundwater quality. Solute transport in the vadose zone is a complex problem because

of the combined effects of soil heterogeneity and the nonlinearity of unsaturated water flow. In the shallow subsurface, the problem is further complicated by the spatial and temporal variability of precipitation and evapotranspiration. Numerical studies in multi-dimensional Gaussian-type heterogeneous soils have shown that solute leaching rates under realistic weather conditions are reduced compared to steadystate conditions, while vertical spreading may either decrease or increase depending on the structure of soil heterogeneity [Russo et al., 1998; Vanderborght et al., 2006]. These phenomena were explained by two underlying processes: i) lateral transport of solute mass into the finer soil matrix during redistribution and upward flow intervals; and ii) a higher downward flow rate during short precipitation events which can either decrease or increase spatial flow variability.

[3] Comparisons between numerical simulations and experimental observations of solute transport in unsaturated heterogeneous porous media with known heterogeneity are essential for supporting numerical studies but are only available for steady-state infiltration conditions [Rossi et al., 2008; Wildenschild, 1999] and they are missing for nonmonotonic transient flow conditions. Recent experiments have confirmed lateral water redistribution within composite porous media from coarse- to fine-grained zones during drying, which may occur over large distances and significantly enhance evaporative losses from heterogeneous porous media compared to homogeneous equivalents [Lehmann and Or, 2009]. The simulation of this lateral redistribution and its effect on solute transport is directly linked to the imposed boundary conditions at the heterogeneous soil surface. Unlike for infiltration events, the definition of boundary conditions for evaporation from heterogeneous soil surfaces is debated [Shokri et al., 2008].

[4] In this study, we present results of two experimental setups. First, salt and dye tracer experiments are used to provide experimental evidence of solute redistribution at the evaporation surface of a composite porous medium. Second, solute redistribution during a full cycle of infiltration and evaporation within and at the evaporation surface of a heterogeneous medium was observed using magnetic resonance imaging (MRI). In contrast to recent evaporation experiments in composite porous media [Lehmann and Or, 2009; Nachshon et al., 2011; Shahraeeni and Or, 2010], we conducted experiments under which the fine and coarse material remained permanently under 'stage-1' (liquid flowdominated) evaporation conditions. Therefore, this study provides indications of solute accumulation in regions at the soil surface that are connected by liquid flow to the deeper soil. Observations were compared with numerical simula-

Copyright 2011 by the American Geophysical Union. 0094-8276/11/2011GL048147

**L17404** 1 of 6

<sup>&</sup>lt;sup>1</sup>Agrosphere Institute, Institute of Bio- and Geosciences, Forschungszentrum Jülich GmbH, Jülich, Germany.

<sup>&</sup>lt;sup>2</sup>Institute of Agricultural Climate Research, Johann Heinrich von Thünen-Institut, Braunschweig, Germany.

<sup>&</sup>lt;sup>3</sup>ITMC, RWTH Aachen University, Aachen, Germany.

<sup>&</sup>lt;sup>4</sup>Department of Hydrology and Water Resources, University of Arizona, Tucson, Arizona, USA.

tions based on common continuum-scale theory for liquid flow and solute transport.

### 2. Materials and Methods

### 2.1. Laboratory Experiments

[5] Laboratory experiments were carried out in coaxial cylindrical quartz sand columns (height: 12.5 cm, diameter d = 8 cm), consisting of a core (d = 2.9 cm) of coarse sand (FH31) surrounded by fine sand (F36) with mean grain sizes of 0.35 and 0.165 mm, respectively (manufacturer: Ouarzwerke Frechen GmbH, Germany). The columns were closed at the bottom by a porous glass filter plate, which remained saturated (saturated conductivity  $K_s = 655$  cm d<sup>-1</sup>) and hydraulically coupled to a reservoir of deionized water. Prior to the experiment, the samples were flushed with deionized water and hydrostatic equilibrium was established with a water table located 19.5 cm below the bottom boundary. We applied 9 ml tracer solution (~ 2 mm water column) manually with a syringe to the surface of the fine sand in four columns. Brilliant Blue (BB) (0.38 wt.%) and KCl (0.6 wt.%) were each used separately as tracers in two of the columns. After tracer application, one column of each pair was covered by a plate to eliminate evaporation, while the others were placed under a fan to create a steady evaporation rate. The evaporation rate was measured continuously by weighing the water reservoirs over a period of 10 days and ranged between 0.7 and 1.0 cm d<sup>-1</sup>. Evaporation rates varied between the columns due to their different position to the fan and varied over time due to air temperature and humidity variations in the lab. No systematic decline in evaporation rate over time was observed so that a nearly steady-state evaporation rate could be assumed. The spatial distribution of the evaporation rate from the heterogeneous soil surface was inferred from surface temperature images obtained with an IR camera (A320, FLIR System). Evaporative cooling resulted in a nearly constant and uniform temperature difference of 3 K between evaporating and non-evaporating columns indicating a uniform evaporation flux from the coarse and fine material. Only the last IR measurement of the evaporating KCl column at day 9 indicated an increase of temperature by 0.5 K in the coarse compared to the fine material. After 10 days, the complete volumes of fine and coarse material were sampled separately and the mass of BB and KCl in each material was determined by leaching the materials with deionized water.

[6] In a second experiment, transport of an MRI contrast agent Gd-DTPA<sup>2-</sup> [Haber-Pohlmeier et al., 2010] was monitored during an infiltration followed by an evaporation phase in an identically prepared sand column. During infiltration, single drip irrigation was applied with a rate of  $3 \text{ cm}^3 \text{ min}^{-1}$ at the center of a porous plate (d = 5 cm) placed on the sample surface and a water table at 1.5 cm below the bottom plate of the column. The hydraulic conductivities of the two materials for this shallow water table were much higher than the infiltration rate, so that the pressure conditions deviated only weakly from hydrostatic equilibrium. When steady flow conditions were reached, 8 cm<sup>3</sup> of a 5 mmol  $1^{-1}$  (0.28 wt.%) Gd-DTPA<sup>2-</sup> solution were applied and flushed with 62 cm<sup>3</sup> of tracer free solution at the same infiltration rate. After irrigation, i.e., 23 minutes after the start of the tracer application, the water table was lowered and maintained as in the first experiment at 19.5 cm below

the bottom boundary. The porous plate was removed from the surface and a fan was operated for 10 days. The evaporation rate, which was measured continuously, ranged between 0.31 and 0.51 cm d<sup>-1</sup> and showed no systematic decline.

[7] Tracer distribution was visualized by collecting high resolution MRI scans using a 4.7 T (200 MHz for <sup>1</sup>H) vertical ultra wide bore magnet (Magnex Scientific, UK), equipped with a Varian gradient system of maximum 300 mT/m and a 170-mm birdcage rf coil. The system was operated by VNMRJ software (Varian, UK). The measurements were performed using a single-echo-multi-slice imaging pulse sequence with strong  $T_1$  weighting ( $t_R = 0.25s$ ,  $t_E = 4.1$ ms, 4 vertical slices of 2mm thickness, FOV: 140x140mm, matrix size 128x128) leading to a nearly linear relation between MRI signal intensity,  $S/S_0$  and the logarithm of the Gd-DTPA<sup>2-</sup> concentration in the range of 0.1–5 mmol 1<sup>-1</sup> [Haber-Pohlmeier et al., 2010]. Above 5 mmol  $1^{-1}$ ,  $S/S_0$ decreases with increasing Gd-DTPA<sup>2-</sup> concentration. Water distribution was determined by the same sequence, but without  $T_1$  weighting and setting  $t_R = 4s$ . The volumetric water content  $\theta$  (cm<sup>3</sup> cm<sup>-3</sup>) maps were calculated from the spatially resolved signal amplitudes. The relative error is about 10% per voxel (e.g.,  $\theta = 0.2 \pm 0.02$ ).

### 2.2. Flow and Transport Modeling

[8] Water flow was described locally by Richards Equation,

$$\frac{\partial \theta(h)}{\partial t} = -\nabla \cdot \theta \mathbf{u} = \nabla \cdot [K(\theta)\nabla h] + \frac{\partial K(\theta)}{\partial z} \tag{1}$$

where t is time (d), h is pressure head (cm),  $\mathbf{u}$  is the pore water velocity vector (cm d<sup>-1</sup>), K is hydraulic conductivity (cm d<sup>-1</sup>) and z is the vertical coordinate directed upwards (cm).  $\theta(h)$  and  $K(\theta)$  were described by the van Genuchten-Mualem (vGM) parametric expressions [van Genuchten, 1980]. Equation (1) was numerically solved with a cell-centered finite-volume code [e.g., Ippisch et al., 2006]. Solute transport was assumed to be governed by the advection-dispersion equation:

$$\theta \frac{\partial C}{\partial t} = -\theta \mathbf{u} \cdot \nabla C + \nabla \cdot (\theta \mathbf{D} \cdot \nabla C) \tag{2}$$

where C is solute concentration in pore water (mmol  $I^{-1}$ ),  $\mathbf{D}$  (cm<sup>2</sup>d<sup>-1</sup>) is the local-scale dispersion tensor of an isotropic porous medium, with  $\mathbf{D} = (\alpha_{\rm T} \| \mathbf{u} \| + D_{\rm m,eff})\mathbf{I} + (\alpha_{\rm L} - \alpha_{\rm T})$   $\mathbf{u}\mathbf{u}^{\rm T} \| \mathbf{u} \|^{-1}$ , where  $\alpha_{\rm T}$  and  $\alpha_{\rm L}$  are the transversal and longitudinal dispersivities (cm), is the effective molecular diffusion coefficient (cm<sup>2</sup> d<sup>-1</sup>), and  $\mathbf{I}$  is the identity matrix. Solute transport was modeled using the random walk particle tracking code PARTRACE [e.g., *Haber-Pohlmeier et al.*, 2010].

[9] The lower boundary of the experiments was described by a prescribed pressure head depending on the imposed water table level. Drip irrigation was modeled as a constant flux by applying the irrigation flow rate uniformly to a circular area surface of 2 cm diameter based on experimental observation (wetted part of the porous plate). Evaporation from the heterogeneous surface was modeled as a uniform flux boundary condition (0.78 cm d<sup>-1</sup> for the BB and KCl experiments and 0.42 cm d<sup>-1</sup> for the Gd-DTPA<sup>2-</sup> experiment), which is supported by IR-derived surface temperature. Simulations were also carried out with lower evaporation rate in the coarse than in the fine material.

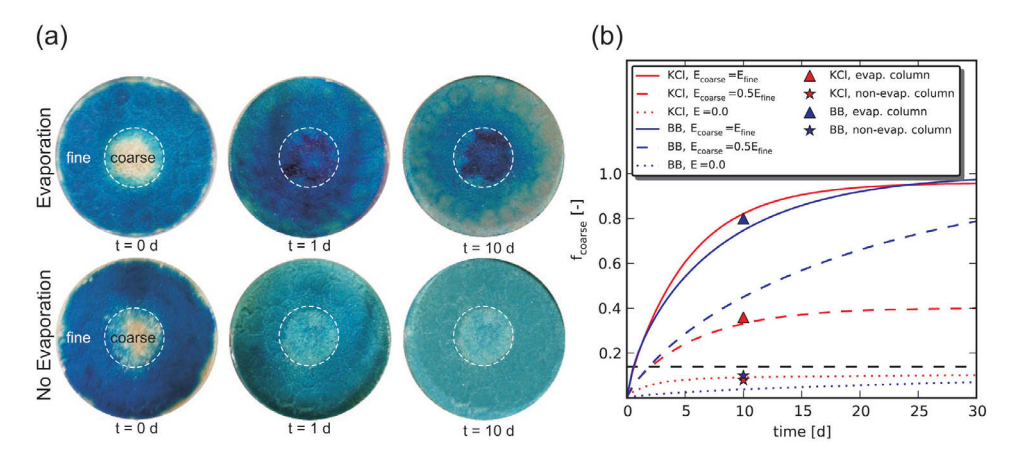


**Figure 1.** (a) Brilliant Blue (BB) experiment. Upper row: column exposed to evaporation. Lower row: covered column, no evaporation. (b) Modeled and measured solute mass fraction in coarse sand  $f_{coarse}$  vs. time after solute application. Black dashed line indicates the evaporating surface fraction of coarse sand. Single data points indicate solute mass fractions determined at the end of the experiment (t = 10 d).

[10] Water flow and solute transport were simulated in three dimensions with a regular grid spacing of 0.1 cm. The hydraulic parameters of the two materials were determined using pressure cells and multi-step outflow experiments (vGM coarse sand:  $\theta_s = 0.4$ ,  $\theta_r = 0.05$ ,  $K_s = 3888$  cm d<sup>-1</sup>,  $\alpha = 0.035 \text{ cm}^{-1}, n = 8.0; \text{ fine sand: } \theta_{\text{s}} = 0.41, \theta_{\text{r}} = 0.05, K_{\text{s}} = 0.05, K_{\text{s}$ 2496 cm d<sup>-1</sup>,  $\alpha = 0.0177$  cm<sup>-1</sup>, n = 10.8). We set the longitudinal dispersivity  $\alpha_{\rm L}$  to the mean grain size and the transverse dispersivity  $\alpha_T = 0.1\alpha_L$ , which are typical values reported for saturated unconsolidated homogenous porous media [Yoon et al., 2008]. The diffusion coefficients  $D_{\rm m}$  of KCl, BB and Gd-DTPA<sup>2-</sup> in water were assumed to be 1.77, 0.086, and 0.35 cm<sup>2</sup> d<sup>-1</sup> [Kasteel et al., 2002; Osuga and Han, 2004], respectively, and were evaluated as a function of water content to obtain  $D_{\rm m,eff}$ :  $D_{\rm m,eff}$ :  $D_{\rm m,eff}$ :  $\theta^{7/3}/\theta_{\rm s}^2$   $D_{\rm m}$  [Millington and Quirk, 1961]. The 3-D model was used to predict the solute concentrations in space and time, which were compared to the MRI results and to the KCl and BB masses that accumulated in the coarse material.

## 3. Results and Discussion

### 3.1. Near-Surface Redistribution of Tracers

[11] The redistribution of BB that was applied at the surface of the fine sand of an evaporating and non evaporating column is shown in Figure 1a. In the column without evaporation, diffusion homogenizes the solute concentration at the soil surface. Diffusion also reduces the concentration at the soil surface due to vertical diffusive mass transport into the soil column as can be derived from decrease of the blue color saturation. In the evaporating column, the dye tracer accumulated during the experiment in the coarse sand whereas the concentration at the surface of the fine sand decreased over time. The decrease in concentration at the surface of the fine sand in the evaporating soil column was not accompanied by a vertical diffusion front that moved downward as in the non-evaporating soil column. The appearance of a thin salt crust in the coarse sand at the end of the experiment of the column to which KCl was applied corroborates the observations of the BB accumulation in the coarse sand. The mass that accumulated in the coarse sand, which makes up 14% of the evaporating surface, was 80%

and 36% of the applied BB and KCl tracer mass, respectively, in the evaporating columns and 10% and 8% of the applied BB and KCl tracer mass, respectively, in the non-evaporating columns. The larger mass fraction of tracer in the coarse material than the evaporating surface fraction of the coarse material implies that mass was transferred by lateral advection fluxes against a concentration gradient from the fine into the coarse sand.

[12] Figure 1b shows the simulated mass accumulation in the coarse sand over time and the observed accumulation after 10 d. The simulated mass accumulation in the coarse sand of the evaporating columns is also larger than the evaporating surface fraction of the coarse sand. This implies that the observed tracer mass transfer from the surface of the fine sand and accumulation at the surface of the coarse sand is in line with classical theory of water flow and solute transport in unsaturated media. However, while the accumulation of BB in the coarse sand of the evaporating column was explained very well by the simulation that assumes uniform evaporation, the accumulation of KCl in the evaporating column was strongly overestimated.

[13] It must be noted that the evaporation fluxes in the coarse and fine material are not predicted by the unsaturated flow equation but are imposed boundary conditions. Based on the uniform surface cooling indicated by IR images, we assumed a uniform evaporation flux. However, due to the relatively small difference in surface temperature between the evaporating and non-evaporating surfaces (3 K), some difference in evaporation rate from the coarse and fine material could have been undetected in the IR surface temperature measurements. Two causes for a lower evaporation rate from the coarse material could be brought forward. First, the rate at which water is removed from the soil surface depends on the vapor pressure at the soil surface, which is close the saturated vapor pressure, and to the resistance to vapor transfer in the air above the soil layer. Recent work of Lehmann and Or that builds on earlier work of Suzuki and Maeda [1968], shows that above drier surfaces of coarse grained materials the resistance to vapor transfer is larger and the evaporation rate smaller than above wetter surfaces of fine grained materials due to larger distances between evaporating micro scale patches. Second,

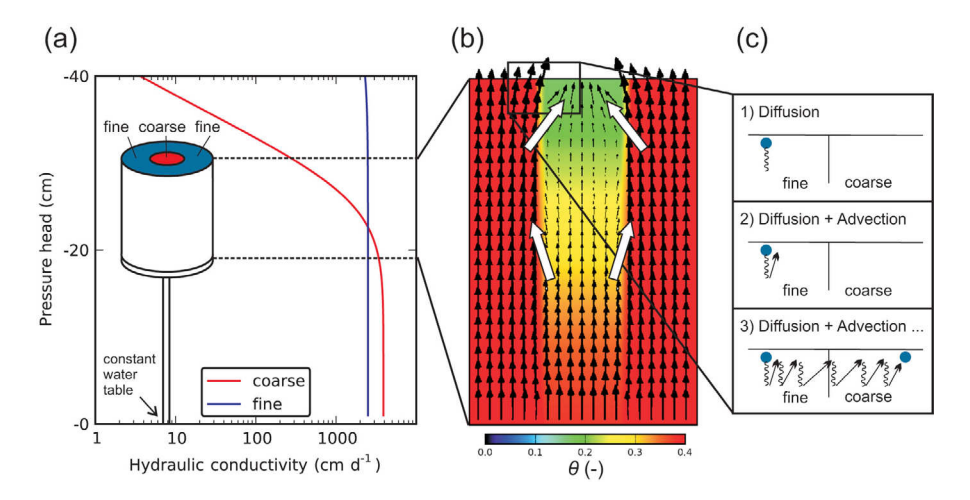


**Figure 2.** (a) Hydraulic conductivity vs. pressure head of the coarse (red) and fine sand (blue). Illustration of the column: Due to the high hydraulic conductivity, pressure head varies almost linearly with depth and deviates little from the hydrostatic equilibrium. (b) Simulated water contents and water flux vectors scaled by magnitude during steady state evaporation. White vectors indicate principal flow direction. (c) Concept of back diffusion and lateral water flow leading to near-surface lateral redistribution and solute mass accumulation.

the increasing osmotic potential of the pore water and the thin salt crust observed at the evaporation surface of the evaporating KCl column may be another reason for a decline in evaporation rate towards the end of the experiment. Therefore, simulations were carried out also for a lower evaporation rate in the coarse sand (0.5 of the evaporation rate from the fine sand). Also for this case, tracer mass accumulation in the coarse sand was simulated (Figure 1b) so that the occurrence of near-surface lateral advective mass transfer and solute accumulation in the coarse sand are not critically dependent on a uniform evaporation rate boundary in the different materials.

[14] Despite the fact that tracer accumulation in the coarse sand must be attributed to a lateral advective flux, also diffusive fluxes play a role in the lateral redistribution process. The smaller molecular diffusion constant of BB compared to KCl leads to larger accumulation of BB at later times, because the simulated back diffusive flux from the coarse material is smaller when the molecular diffusion constant is smaller. The effect of back diffusion is enhanced when the lateral advective fluxes into the coarse material are decreased due to a lower evaporation rate from the coarse material in the evaporating KCl column towards the end of the experiment together with back diffusion could explain the lower experimental accumulation of KCl compared to BB.

[15] To obtain better insight in the processes leading to near surface lateral redistribution, the hydraulic conductivities of the two materials at the different heights, simulated water contents, and water flux vectors during the steady state evaporation are shown in Figures 2a and 2b. Above –11cm height in the soil column, the fine sand is more conductive than the coarse sand. This leads to a lateral redistribution of water from the coarse into the fine sand between –11 cm and –2 cm height and to a lower upward flux in the coarse sand than in the fine sand. Imposing a uniform evaporative demand, lateral flow back from the fine into the coarse sand close to the sample surface between –2

and 0 cm height must compensate for the lower upward flux in the coarse sand deeper in the sample. The simulated surface water content in the coarse sand of  $\theta=0.17$  and its near-surface unsaturated hydraulic conductivity of 110 cm d<sup>-1</sup> were still high enough to ensure liquid phase continuity and the lateral fluxes that sustain the evaporative demand from the coarse sand with relatively low hydraulic gradients. In addition to the uniform IR surface temperatures and uniform evaporative cooling, the fact that the coarse sand surface did not consist of loose sand particles is an additional indication that also in the experiment liquid films and water menisci that keep particles together and ensure liquid phase continuity were present.

[16] Representing solute diffusion by random particle displacements can be used to illustrate the accumulation of solutes in the coarse material (Figure 2c). When solutes at the evaporating surface of the fine sand are moved downwards by diffusion against the upward evaporative flux, the lateral component of the advective flux will result in a net lateral solute flux from the fine towards the coarse material.

#### 3.2. Redistribution of Tracers Deeper in the Sample

[17] Figure 3 shows MRI observed and simulated water content and MRI signal intensities S/S<sub>0</sub>, which are between 0.3 and 0.8 proportional to the logarithm of Gd-DTPA<sup>2-</sup> concentration, during an infiltration-evaporation cycle in the composite medium. During the infiltration phase, high pressure heads caused a nearly uniform water content distribution in the sample with small variability being related to packing inhomogeneities and lower MRI sensitivity at the top and bottom of the sample (Figure 3a). Under these conditions, hydraulic conductivity was highest in the inner core filled with coarse sand. The infiltration phase was characterized by fast transport in the coarse sand, while lateral flow away from the drip source and dispersive spreading moved part of the tracer plume into the fine sand (Figure 3b, t = 2 min). The lowering of the water table between infiltration and evaporation phase caused drainage

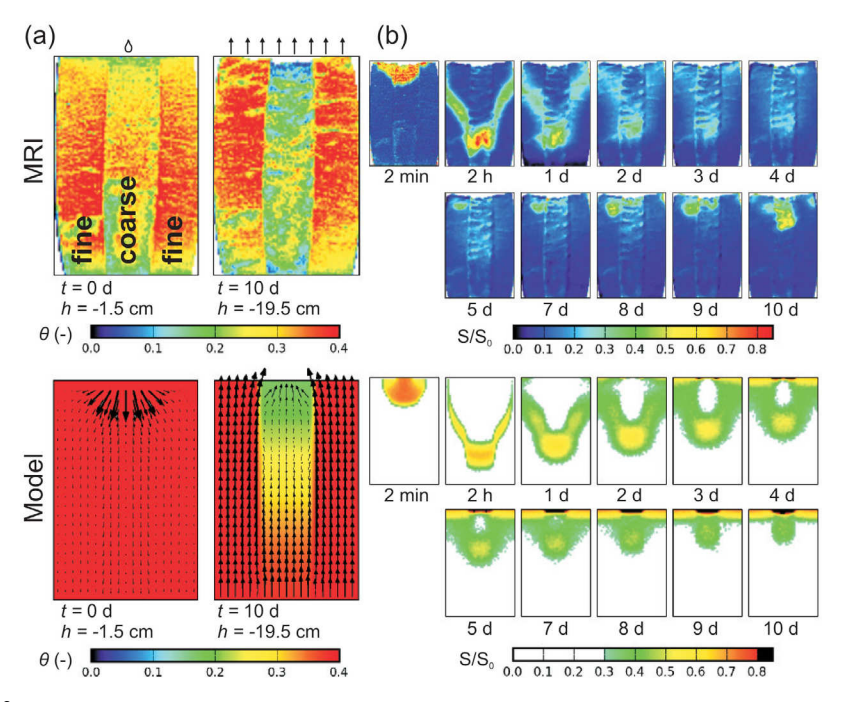


**Figure 3.** Gd-DTPA<sup>2-</sup> tracer experiment. Shown is a vertical slice through the center of the column. (a) (top) Water content derived from MRI during infiltration and evaporation phase. (bottom) Modeled water content and flow vectors scaled by magnitude. (b) MRI Signal intensity  $S/S_0$  that is proportional to logarithm of the Gd-DTPA<sup>2-</sup> concentration; (top) derived from MRI, (bottom) derived from simulated Gd-DTPA<sup>2-</sup> concentration.

mainly from the coarse sand which moved the tracer plume down in the coarse sand (Figure 3b, t = 2 h). The lowering of the water table and the change of the flow direction provoked a change of the flow pattern. Both experiment and simulation show that mass accumulated more rapidly at the soil surface in both the fine and coarse material than that the plume in the coarse material moved upward so that the zone between the tracer plume in the coarse material and the soil surface seems to be bypassed by the tracer (Figure 3b, days 1-5). This suggests that deeper in the soil profile, tracer was transported from the coarse to the fine material, in which the upward flux was higher. The simulations indicate that lateral redistribution continues when most of the tracer mass is at the soil surface and leads to a depletion of tracer in the fine sand and an accumulation in the coarse sand (Figure 3b, days 8-10). The simulations also indicate that the accumulation leads to a zone of high tracer concentrations in a shallow layer below the soil surface that exceeds the concentration range with a positive correlation between tracer concentration and S/S<sub>0</sub>. However, the increase in S/S<sub>0</sub> deeper below the surface in the coarse sand combined with a decrease in the fine zone between day 8 and 10 indicates a near surface lateral redistribution of the tracer mass in the experiment. This increase at a greater depth could have been caused by density-driven downward transport, which is ignored in the model. The removal of the infiltration disk and the sand that stack to it disturbed the coarse sand surface, caused a lower packing density, lower water contents close to the soil surface and a local depression of the evaporating surface in the coarse sand which was a few mm lower than the evaporating surface of the fine sand. This depression may have caused a lower evaporation rate from

the coarse sand and less lateral redistribution of tracer mass close to the surface.

### 4. Conclusions

[18] We presented experimental evidence of solute redistribution at the wet surface of a composite porous medium during evaporation. The observations were well reproduced by numerical simulations based on Richards' equation and advection-dispersion equation. One key result of the redistribution process was the accumulation of solutes in coarsegrained zones near the sample surface. For evaporating wet surfaces that are connected by liquid films to the deeper soil, the results of this study indicate that solute accumulation may be largely decoupled from the local evaporation fluxes and rather be governed by the relative differences of the hydraulic conductivities, the scale of the heterogeneity, and the diffusion coefficient and solubility of the dissolved substance. Molecular diffusion that moves solutes away form the evaporating surface back into the porous medium in combination with lateral water flow will redistribute and accumulate solutes towards locations with the lowest hydraulic head, i.e., the lowest sum of pressure and gravitational head. These locations correspond to regions with low hydraulic conductivity, which can be either fine- or, like in our experiments, coarse-grained regions, depending on the capillary pressure conditions. Using simulations, we showed that locations where solutes accumulate need not be locations with the highest local evaporation.

[19] The results obtained in this study are different from salt accumulation that was observed in evaporation experiments of successively drying composite porous media [Lehmann and Or, 2009; Nachshon et al., 2011; Shahraeeni

and Or, 2010]. In these experiments part of the evaporating soil surface dried out and was not connected by liquid flow to the deeper soil. Evaporation from the dried out part of the surface was dominated by vapor flow in the porous medium. When a soil surface consists of dry regions dominated by vapor-flow and wet regions dominated by liquid-flow to the soil surface, solute accumulation takes place at the surface of the liquid-flow dominated region, i.e., the fine region, where the evaporation rate is higher. The comparison of our results with the previous experiments indicates that solute redistribution and locations of solute accumulation on a heterogeneous surface depends on the state of the surface. Since the soil surface state changes dynamically, it is therefore not possible to make generally valid statements about salt accumulation on heterogeneous soil surfaces.

[20] The accumulation of solutes at the surface of coarser regions that are usually preferential flow pathways during strong precipitation may have an accelerating effect on the leaching of solutes. Where and whether redistribution occurs depends on the timing and duration of leaching and evaporation periods after solute application. This lends further importance to understanding the dynamics of boundary conditions, complementing effects such as macropore flow activation during infiltration. Future research should investigate the impacts of heterogeneity during infiltration and evaporation across a range of soil structures and boundary conditions, perhaps leading to an effective parameter model that can account for the small-scale redistribution processes at larger scales.

- [21] **Acknowledgments.** We thank Patrick Wünnemann from Aachen university and Dagmar van Dusschoten of the Eco-NMR center at the IBG-3 (Forschungszentrum Jülich) for their help during the MRI measurements, and Odilia Esser for the dye analysis. Jan Vanderborght would like to acknowledge the DFG funded research project Multi-scale Interfaces in Unsaturated Soil (MUSIS, FOR 1083).
- [22] The Editor thanks the anonymous reviewer for their assistance in evaluating this paper.

### References

- Haber-Pohlmeier, S., M. Bechtold, S. Stapf, and A. Pohlmeier (2010), Water flow monitored by tracer transport in natural porous media using magnetic resonance imaging, *Vadose Zone J.*, 9(4), 835–845, doi:10.2136/vzj2009.0177.
- Ippisch, O., H. J. Vogel, and P. Bastian (2006), Validity limits for the van Genuchten-Mualem model and implications for parameter estimation and numerical simulation, Adv. Water Resour., 29(12), 1780–1789, doi:10.1016/j.advwatres.2005.12.011.

- Kasteel, R., H. J. Vogel, and K. Roth (2002), Effect of non-linear adsorption on the transport behaviour of Brilliant Blue in a field soil, Eur. J. Soil Sci., 53, 231–240, doi:10.1046/j.1365-2389.2002.00437.x.
- Lehmann, P., and D. Or (2009), Evaporation and capillary coupling across vertical textural contrasts in porous media, *Phys. Rev. E*, 80(4), 046318, doi:10.1103/PhysRevE.80.046318.
- Millington, R., and J. P. Quirk (1961), Permeability of porous solids, *Trans. Faraday Soc.*, 57(8), 1200–1207, doi:10.1039/tf9615701200.
- Nachshon, U., N. Weisbrod, M. I. Dragila, and A. Grader (2011), Combined evaporation and salt precipitation in homogeneous and heterogeneous porous media, *Water Resour. Res.*, 47, W03513, doi:10.1029/2010WR009677.
- Osuga, T., and S. Han (2004), Proton magnetic resonance imaging of diffusion of high- and low molecular-weight contrast agents in opaque porous media saturated with water, *Magn. Reson. Imaging*, 22(7), 1039–1042, doi:10.1016/j.mri.2003.07.004.
- Rossi, M., O. Ippisch, and H. Flühler (2008), Solute dilution under imbibition and drainage conditions in a heterogeneous structure: Modeling of a sand tank experiment, *Adv. Water Resour.*, *31*(9), 1242–1252, doi:10.1016/j.advwatres.2008.04.003.
- Russo, D., J. Zaidel, and A. Laufer (1998), Numerical analysis of flow and transport in a three-dimensional partially saturated heterogeneous soil, *Water Resour. Res.*, 34(6), 1451–1468, doi:10.1029/98WR00435.
- Shahraeeni, E., and D. Or (2010), Thermo-evaporative fluxes from heterogeneous porous surfaces resolved by infrared thermography, *Water Resour. Res.*, 46, W09511, doi:10.1029/2009WR008455.
- Shokri, N., P. Lehmann, P. Vontobel, and D. Or (2008), Drying front and water content dynamics during evaporation from sand delineated by neutron radiography, *Water Resour. Res.*, 44, W06418, doi:10.1029/ 2007WR006385.
- Suzuki, M., and S. Maeda (1968), On the mechanism of drying granular beds: Mass transfer from discontinuous source, *J. Chem. Eng. Jpn.*, *I*(1), 26–31, doi:10.1252/jcej.1.26.
- van Genuchten, M. T. (1980), A closed-form equation for predicting the hydraulic conductivity of unsaturated soils, *Soil Sci. Soc. Am. J.*, 44(5), 892–898, doi:10.2136/sssaj1980.03615995004400050002x.
- Vanderborght, J., R. Kasteel, and H. Vereecken (2006), Stochastic continuum transport equations for field-scale solute transport: Overview of theoretical and experimental results, *Vadose Zone J.*, 5(1), 184–203, doi:10.2136/vzj2005.0024.
- Wildenschild, D. Y. Y. (1999), Numerical modeling of observed effective flow behavior in unsaturated heterogeneous sands, *Water Resour. Res.*, 35(1), 29–42, doi:10.1029/98WR01959.
- Yoon, H., C. Y. Zhang, C. J. Werth, A. J. Valocchi, and A. G. Webb (2008), Numerical simulation of water flow in three dimensional heterogeneous porous media observed in a magnetic resonance imaging experiment, *Water Resour. Res.*, 44, W06405, doi:10.1029/2007WR006213.
- M. Bechtold, A. Pohlmeier, J. Vanderborght, and H. Vereecken, Agrosphere Institute, Institute of Bio- and Geosciences, Forschungszentrum Jülich GmbH, Leo-Brandt-Strasse, D-52425 Jülich, Germany. (michel. bechtold@vti.bund.de)
- T. P. A. Ferré, Department of Hydrology and Water Resources, University of Arizona, Tucson, AZ 85721-0011, USA.
- S. Haber-Pohlmeier, ITMC, RWTH Aachen University, D-52074 Aachen, Germany.